CMAME-D-22-01095 Revision notes

A novel stabilized NS-FEM formulation for anisotropic double porosity media

Qi Zhang[1], Ze-Yu Wang[1], Zhen-Yu Yin[1], and Yin-Fu Jin[1,2]

[1]Department of Civil and Environmental Engineering, The Hong Kong Polytechnic University, Hung Hom, Kowloon, Hong Kong, China
[2]College of Civil and Transportation Engineering, Shenzhen University, Shenzhen, China

The reviewers' comments have been listed in order below in *italic* text, followed by responses in normal text. All the revised parts have been highlighted in the revised manuscript. Thank you again for your comments and suggestions, which have greatly improved the manuscript.

Reviewer 1

Q 1.1 *In this work, an anisotropic poroelastic relation was derived in a similar thought experiment manner, as previously developed by James Berryman, Jihoon Kim, and Amin Mehrabian. Next, the elastoplastic tensor $\mathbb{C}^{ep}$ is incorporated in a heuristic way. To solve the IBVP accurately and efficiently by using FEM, node-based smoothed-FEM (on linear triangle element) with modified nodal integration and PPP was proposed in the residual form. Six numerical examples are given subsequently. To demonstrate that the "MNI" and "STAB" terms are effective, relevant parameter settings are described, and convincing results are presented. The unique characteristics in double porosity media are also reported. However, some problems still need to be addressed in the revised submission. The specific comments are given as follows.*

Reply: Thank you for the nice summary about our work. Our detailed responses are given below.

Q 1.2 *Since the authors have proposed a new anisotropic poroelastic relation for double porosity media, the reviewer wonders whether this method can be extended to multiple porosity media? Because if the extension can be done analogously, this work will benefit the numerical simulation of multiple porosity media.*

Reply: Thank you for your nice comment. The proposed formulation can be perfectly generalized to the case of multiple porosity. In multiple porosity media, N materials (constituents) are characterized by $v^{[l]}$, $\mathbb{S}^{[l]}$, $\boldsymbol{B}^{[l]}$, $\boldsymbol{\alpha}^{[l]}$, and $D^{[l]}$ ($l = 1, 2, \ldots, N$). They are assumed to be anisotropic in the most general case. The macroscopic poroelastic equation for the whole mixture is simply a natural extension of (12) in the current work, which may be written as

$$\begin{bmatrix} \mathbf{Vec}\,(\boldsymbol{e}) \\ \zeta_1 \\ \vdots \\ \zeta_N \end{bmatrix} = \begin{bmatrix} \mathbf{Mat}\,(\mathbb{S}^*) & a_1 & \cdots & a_N \\ a_1^T & d_{11} & \cdots & d_{1N} \\ \vdots & \vdots & \ddots & \vdots \\ a_N^T & d_{N1} & \cdots & d_{NN} \end{bmatrix} \begin{bmatrix} \mathbf{Vec}\,(\boldsymbol{\sigma}) \\ p_1 \\ \vdots \\ p_N \end{bmatrix}. \tag{1}$$

The same strain compatibility relation $\mathbf{Vec}\,(\boldsymbol{e}) = \sum_{k=1}^{N} v^{[k]}\,\mathbf{Vec}\left(\boldsymbol{e}^{[k]}\right)$ and the uniform confining stress condition are applied next, in order to derive the coefficients in Eq. (1). The results read ($l = 1, 2, \ldots, N$)

$$\mathbf{Mat}\,(\mathbb{S}^{*}) = \sum_{k=1}^{N} v^{[k]}\,\mathbf{Mat}\left(\mathbb{S}^{[k]}\right)\,, \tag{2}$$

$$a_l = \frac{1}{3} v^{[l]} D^{[l]}\,\mathbf{Vec}\left(\boldsymbol{B}^{[l]}\right)\,, \tag{3}$$

$$d_{ll} = v^{[l]} D^{[l]}\,. \tag{4}$$

Note all the off-diagonal terms d_{ij} $(i \neq j)$ are zero (Kim et al., 2012). Equation (1) can be rewritten in the mixed stiffness form by exchanging the position of $\boldsymbol{e}$ and $\boldsymbol{\sigma}$, which would give the familiar Biot tensors and storage coefficients. The pure stiffness form is obtained by inverting the matrix in Eq. (1).

We want to add a further remark about the strain compatibility relation and the uniform confining stress condition. These two conditions can be visually obtained from the equivalence of the potential energy density. In other words, the energy density of the multiple porosity material U must be equal to the weighted sum of the individual constituents' energy density U_i. This can be expressed mathematically as

$$U = \sum_{i=1}^{N} v^{[i]} U_i\,, \tag{5}$$

$$U = \frac{1}{2}\left(\boldsymbol{\sigma} : \boldsymbol{e} + \sum_{i=1}^{N} \zeta_i p_i\right)\,, \tag{6}$$

$$U_i = \frac{1}{2}\left(\boldsymbol{\sigma}^{[i]} : \boldsymbol{e}^{[i]} + \bar{\zeta}_i p_i\right)\,. \tag{7}$$

Note that $\zeta_i = v^{[i]}\bar{\zeta}_i$ in which ζ_i represents the global fluid content variation and $\bar{\zeta}_i$ represents the local fluid content variation.

The revised content could be found in Appendix A.

Q 1.3 *The authors failed to describe the return mapping algorithm of the strain-softening Drucker-Prager model. How do you deal with the softening functions of cohesion and internal friction angle?*

Reply: Thank you for your comment. The algorithm is given as follows. For simplicity, $\boldsymbol{\sigma}$ is used to represent the effective stress tensor of solid as that in solid mechanics. That is to say, please interpret it as $\boldsymbol{\sigma}''$ in the hydromechanical coupling analysis.

Step 1. Compute the following quantities

$$\boldsymbol{\sigma}^{\mathrm{tr}} = \boldsymbol{\sigma}_n + \mathbb{C}^{e} : \Delta\boldsymbol{\epsilon}\,,$$

$$p^{\mathrm{tr}} = \frac{\mathrm{Tr}\,(\boldsymbol{\sigma}^{\mathrm{tr}})}{3}\,,$$

$$\boldsymbol{s}^{\mathrm{tr}} = \boldsymbol{\sigma}^{\mathrm{tr}} - p^{\mathrm{tr}}\mathbf{1}\,,$$

$$q^{\mathrm{tr}} = \sqrt{\frac{3}{2}}\,\|\boldsymbol{s}^{\mathrm{tr}}\|\,,$$

$$\hat{\boldsymbol{n}} = \frac{\boldsymbol{s}^{\mathrm{tr}}}{\|\boldsymbol{s}^{\mathrm{tr}}\|}\,.$$

Step 2. The yield function of the Drucker-Prager plasticity is of the form

$$\tilde{f}(x,y) = \sqrt{\frac{2}{3}}y + Bx - A\,,$$

where A and B are two material parameters, and they are functions of cohesion c and friction angle ϕ. One possible choice is by making the Drucker-Prager yield surface inscribe the Mohr-Coulomb yield surface, which yields

$$A = \frac{3\sqrt{2}c\cos\phi}{\sqrt{9+3\sin^2\phi}}\,,$$

$$B = \frac{3\sqrt{2}\sin\phi}{\sqrt{9+3\sin^2\phi}}\,.$$

We also define another parameter b in an analogous manner as

$$b = \frac{3\sqrt{2}\sin\psi}{\sqrt{9+3\sin^2\psi}}\,,$$

where $\psi \leq \phi$ is the dilatancy angle. Now we check the sign of $\tilde{f}(p^{\text{tr}}, q^{\text{tr}})$. For a positive number, we would proceed to step 3. Otherwise, the final stress $\boldsymbol{\sigma} = \boldsymbol{\sigma}^{\text{tr}}$ and algorithm is terminated (c and ϕ remain the same, the algorithmic stress-strain tangent operator is $\mathbb{C}^e$).

Step 3. Calculate the discrete plastic multiplier $\Delta\lambda$ as (Borja, 2013)

$$\Delta\lambda = \frac{\sqrt{2/3}q^{\text{tr}} + Bp^{\text{tr}} - A}{2\mu + BKb}\,,$$

where K is the bulk modulus and μ is the shear modulus used to construct $\mathbb{C}^e$. Note that this equation for $\Delta\lambda$ is only correct for isotropic elastoplasticity. For anisotropic elastoplasticity, a closed-form solution of $\Delta\lambda$ may not be easy to obtain.

Step 4. Compute the final stress $\boldsymbol{\sigma}$ and update c, ϕ, and ψ (or equivalently: A, B, and b) by using the softening law (52)(53) of the manuscript (copied here for easy reference) according to the new equivalent (deviatoric) plastic strain ε^p_{eq}

$$\boldsymbol{\sigma} = \boldsymbol{\sigma}^{\text{tr}} - \Delta\lambda\left(Kb\mathbf{1} + 2\mu\hat{\boldsymbol{n}}\right)\,,$$

$$\varepsilon^p_{eq} = \left(\varepsilon^p_{eq}\right)_n + \sqrt{\frac{2}{3}}\Delta\lambda\,.$$

$$\phi = \psi = \phi_r + \left(\phi_p - \phi_r\right)\exp\left(-\eta\varepsilon^p_{eq}\right)\,,$$

$$c = c_r + \left(c_p - c_r\right)\exp\left(-\eta\varepsilon^p_{eq}\right)\,,$$

The algorithmic stress-strain tangent operator is ($\mathbb{I}$ is the symmetric fourth-order identity tensor)

$$\mathbb{c} = \mathbb{C}^e - \left(Kb\mathbf{1} + 2\mu\hat{\boldsymbol{n}}\right)\otimes\frac{2\mu\hat{\boldsymbol{n}} + BK\mathbf{1}}{2\mu + BKb} - \frac{4\mu^2\Delta\lambda}{\|\boldsymbol{s}^{\text{tr}}\|}\left(\mathbb{I} - \frac{1}{3}\mathbf{1}\otimes\mathbf{1} - \hat{\boldsymbol{n}}\otimes\hat{\boldsymbol{n}}\right)\,.$$

The revised content could be found in Appendix C.

Q 1.4 *A brief discussion on the determination of the PPP coefficient is suggested. In Sun et al. (2013), another pore pressure stabilization method was developed, which is still popular nowadays. How do you compare these two methods?*

Reply: Thank you for your comment. Sun et al. (2013) proposed an automatic estimation technique of stabilization parameter τ for single porosity geomechanics, which considers the compressibility of fluid and solid grains, and the variation of time step and mesh size. Because the dimensionless time of one-dimensional consolidation $\hat{t} = c_v t / h^2$ plays a central role in this equation, which also controls the generation/dissipation of excess pore pressure, Sun's proposal could be more physically sound than a constant stabilization parameter that needs trial and error. Nevertheless, $\tau = 2$ always works in our numerical examples, and Sun's proposal based on a 1D problem cannot be always relied upon as a definitive analytical solution for the optimal value of the stabilization parameter.

The revised content could be found in the paragraph after Eq. (51).

Q 1.5 *The strain localization phenomenon is significant in your last two examples. Does the problem of mesh-dependency still exist for your proposed method? If yes, what measures can be taken to circumvent this problem?*

Reply: Thank you for your comment. Yes, we have checked that the problem of mesh-dependency still exists for our proposed method. To circumvent this problem, the Cosserat continuum theory is a feasible approach, and we are currently trying to incorporate it into the framework of SFEM. Nevertheless, for the same mesh size, the strain localization is not very sensitive to the distortion of mesh, as shown in Figure 15 of Wang et al. (2022).

Q 1.6 *One of the advantages of the proposed method is its computational efficiency, since it takes advantage of "linear shape function and its piecewise constant derivatives". The proposed method will lose this advantage regarding the potential of extension to 3D or using higher-order interpolations. Therefore, what makes the proposed method superior to the other coupled FE models?*

Reply: Thank you for your comment. For node-based smoothed FEM, although the higher order interpolations can be considered, the linear interpolation is still the most popular choice and also gives the high accuracy compared to high order interpolations, shown in Feng et al. (2016). One of the most appealing advantages of S-FEM is the use of low-order element to give accurate solution with high efficacy (Zeng and Liu, 2018). For the 3D extension of SNS-PFEM with PPP, the 4-node linear tetrahedron element (T4) will be adopted, same as the study of Yang et al. (2019). The T4 element shares many essential mathematical features with T3 element, so it can be anticipated that most of the numerical features in this manuscript can be preserved in the 3D conditions.

Q 1.7 *Following my previous comment, could you give some quantitative results to demonstrate computational efficiency?*

Reply: Thank you for your comment. As for the amount of computation, Figure 13 of Wang et al. (2022) already illustrates the computational efficiency of NS-FEM, compared with the standard FEM. The NS-FEM has the lowest computational time while the results accuracy is still as good as the traditional FEM, as shown in Figure 9 of Wang et al. (2022). Similar characteristics are also preserved in our examples.

Q 1.8 *In terms of the solid constitutive model, is it possible to incorporate a time-dependent plasticity model, say a viscoplastic model, into the hydromechanical simulation using your proposed numerical scheme?*

Reply: Thank you for your comment. Yes, the proposed numerical scheme can be applied to geotechnical practice with advanced soil models. To show this capability, we conducted a series of simulations to predict the long-term settlement of embankment with an advanced soil model abbreviated as ANICREEP proposed by Yin et al. (2011). In the simulation, the permeability changes with the void ratio in a double

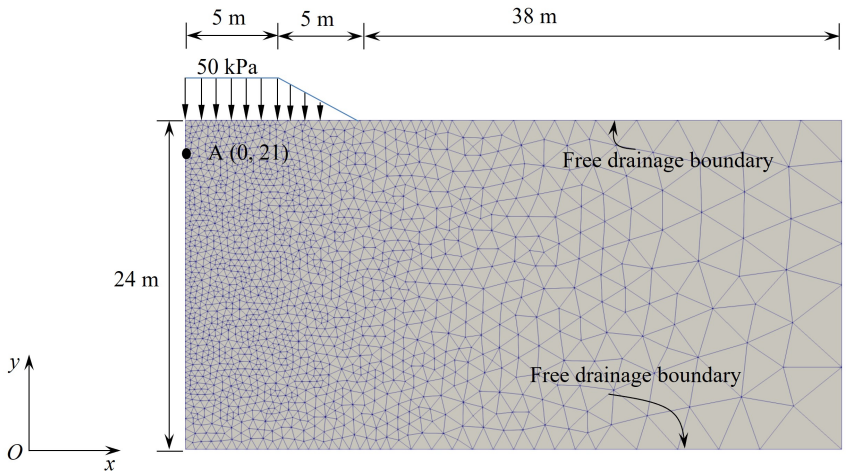

Figure 1: Geometry of embankment.

Figure 2: Distribution of the void ratio at the end of the simulation.

log-linear relationship, same as that adopted in PLAXIS. Self-weight is also included in the simulation. Some preliminary results can be found as follows.

Q 1.9 *It is surprising to find that in your 1D consolidation case, the pressures predicted by the two systems are NOT the same in the undrained limit, while this is not the case in Zhao and Borja (2021) Eq. (99a) to Eq. (102). How do you explain this difference?*

Reply: Thank you for your comment. In the undrained limit as $\Delta t \to 0$, only terms involving solid deformation and storage coefficients survive, which means that we are effectively solving the following equations

$$\boldsymbol{\alpha}_1 : \frac{\mathrm{d}\boldsymbol{e}}{\mathrm{d}t} + A_{11}\frac{\mathrm{d}p_1}{\mathrm{d}t} + A_{12}\frac{\mathrm{d}p_2}{\mathrm{d}t} = 0\,, \tag{8}$$

$$\boldsymbol{\alpha}_2 : \frac{\mathrm{d}\boldsymbol{e}}{\mathrm{d}t} + A_{12}\frac{\mathrm{d}p_1}{\mathrm{d}t} + A_{22}\frac{\mathrm{d}p_2}{\mathrm{d}t} = 0\,. \tag{9}$$

Above two equations suggest that only some particular combinations of these coefficients may lead to $p_1 = p_2$ in the undrained limit. In order to derive these particular combinations, an assumption is made on

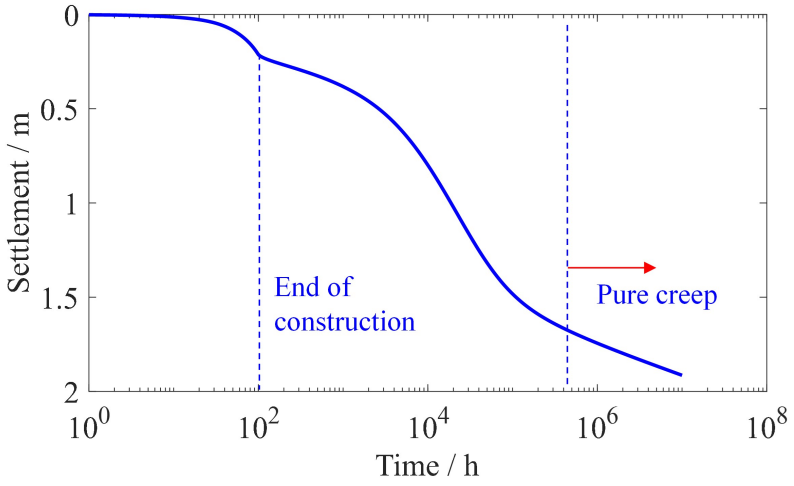

Figure 3: Evolution of surface settlement.

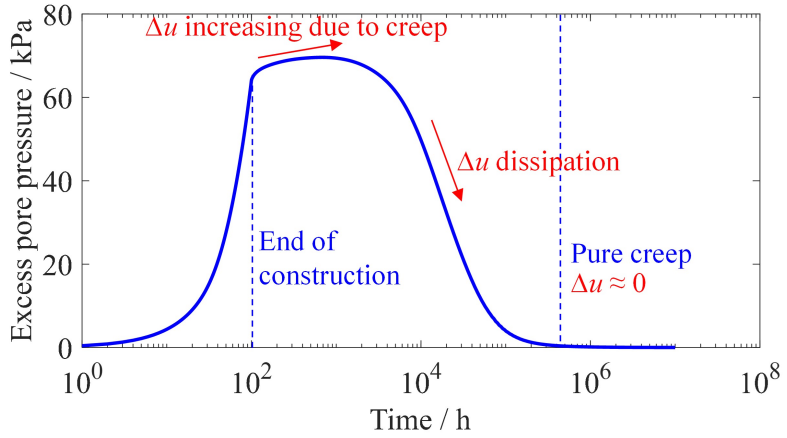

Figure 4: Evolution of excess pore water pressure at point A.

$\boldsymbol{\alpha}_1$ and $\boldsymbol{\alpha}_2$ such that they can be represented as scalars multiplied by the same second-order tensor. Let us denote this second-order tensor as $\mathbf{a}$, thus $\boldsymbol{\alpha}_1 = b_1\mathbf{a}$ and $\boldsymbol{\alpha}_2 = b_2\mathbf{a}$ where b_1 and b_2 are scalars. Next we multiply Eq. (8) with b_2 and Eq. (9) with b_1 and take the difference, the result is

$$(A_{11}b_2 - A_{12}b_1)\frac{\mathrm{d}p_1}{\mathrm{d}t} + (A_{12}b_2 - A_{22}b_1)\frac{\mathrm{d}p_2}{\mathrm{d}t} = 0\,. \tag{10}$$

The condition of $p_1 = p_2$ would require the coefficient of $\mathrm{d}p_1/\mathrm{d}t$ is to the opposite of the coefficient of $\mathrm{d}p_2/\mathrm{d}t$, which can be rearranged as

$$(A_{11} + A_{12})\,b_2 = (A_{12} + A_{22})\,b_1\,. \tag{11}$$

In Zhao and Borja (2021), their storage coefficients satisfy Eq. (11), while in our third verification example, the coefficients do not satisfy Eq. (11). That is the reason why the undrained responses in two papers are different. For our third verification example, the undrained pressures can be analytically calculated as shown in Eqs. (53)(54) of Zhang et al. (2021).

Q 1.10 *It would be better to have a detailed calculation spreadsheet with real numbers of Section 2.2. From this spreadsheet, could you explain the large discrepancy between Berryman's effective stress coefficients and Borja's effective stress coefficients, as discovered by Zhang and Borja (2021)?*

Reply: Thank you for your comment. We have added a new section to illustrate the use of formulas and explain the large discrepancy between different effective stress coefficients. Please refer to Section 3 for revised details.

The revised content could be found in Section 3.

Q 1.11 *The mesh sizes of numerical examples should be given to make the description more complete.*

Reply: Thank you for your comment. The information about the mesh size has been added.

Reviewer 2

Q 2.1 *In this work, the authors proposed a novel poroelastoplastic formulation for anisotropic double porosity media. The proposed method has been validated through a series of examples with benchmark solutions. This paper is very well written and the proposed formulation is novel. The reviewer recommends the paper be accepted with some minor revisions.*

Reply: Thank you for the nice summary about our work. Our detailed responses are given below.

Q 2.2 *The derivations of the proposed constitutive formulation (Section 2) and NS-FEM formulation (Section 3) are very lengthy. It is not easy to keep track of all assumptions the authors make when extending the existing theories. It would be beneficial to include tabular or itemized lists summarizing key model assumptions and how one can recover existing isotropic forms for (1) the proposed anisotropic double porosity constitutive form; (2) extension of the stabilized NS-FEM formulation.*

Reply: Thank you for your comment. Yes, a summary of the key model assumptions will be helpful. Please refer to Section 2.1 and Section 4 for revised details.

The revised contents could be found in Section 2.1 and Section 4.

Q 2.3 *The implementation of the governing equations (e.g., Eqs. (27)(28) with the proposed constitutive laws) is a non-trivial task. Where has the proposed framework been implemented? The analytical expression of the algorithmic tangent operator is also complicated. It would be beneficial to include more details in either Appendix or as supplemental materials.*

Reply: Thank you for your comment. The proposed framework has been implemented in MATLAB to form our own in-house SFEM code simulator. The FEM mesh is based on a well-established generator called MESH2D, through which the coordinate of each node and connectivity of each element are obtained. Subsequently, the smoothing operation is applied to compute adjacent elements of each node, the smoothing domains, and sub-domains, which would enable the calculation of smoothed matrices from corresponding compatible matrices. Constant "stiffness" matrices, MNI terms, and PPP terms are pre-calculated before the main solving process. During the main solving process, only the contribution from constitutive model at each node will be assembled, other calculations are purely sparse matrix and vector multiplications. A "save state" function saves some history variables for next time step and plotting. A post-processing module is given in the end. We have made our code publicly available from this GitHub page under the **Releases** menu.

As for the analytical expression of the algorithmic tangent operator, we have added more details in the revised version. The details of the Drucker-Prager model are given in Appendix C; while the details of the AMCC model are given in a separate supplementary document because it will be too long if including the details in the appendix. The main difference between these two algorithms is that a closed-form solution of discrete plastic multiplier $\Delta\lambda$ does not exist for AMCC, so another loop of Newton's method is necessary.

The revised contents could be found in Appendix C and the supplementary document.

Q 2.4 *For validation examples, it is not clear to the reviewer if all parameters used (e.g., Tables 1-4) are taken from the cited references or if there are any model parameters unique to the proposed constitutive form that require calibration or tuning.*

Reply: Thank you for your comment. For the first three verification examples, the parameters are taken from the cited references. In particular, the five elastic constants of a transversely isotropic Trafalgar shale used in the first example are converted from measured undrained constants (it would be impractical to wait for the shale to be fully drained), as given in 5.5 of Cheng (2016). For the last example, the AMCC parameters are calibrated with the experimental data on Tournemire shale, and this calibration process is given in Zhao et al. (2018). Here we just borrow their parameters and test the effectiveness of SFEM on the same boundary-value problem.

Q 2.5 *Figure 21, even if cases 1-3 overlap, it would still be good to distinguish them with three different line types.*

Reply: Thank you for your comment. The new figure is shown here (Figure 5). However, in the revised manuscript, we dropped this figure because it is not very interesting and also did not show the characteristic of double porosity media. The curves for Cases 1-3 are somehow similar to Figure 16 in Wang et al. (2022) by using a Mohr-Coulomb model with strain-softening for single porosity media.

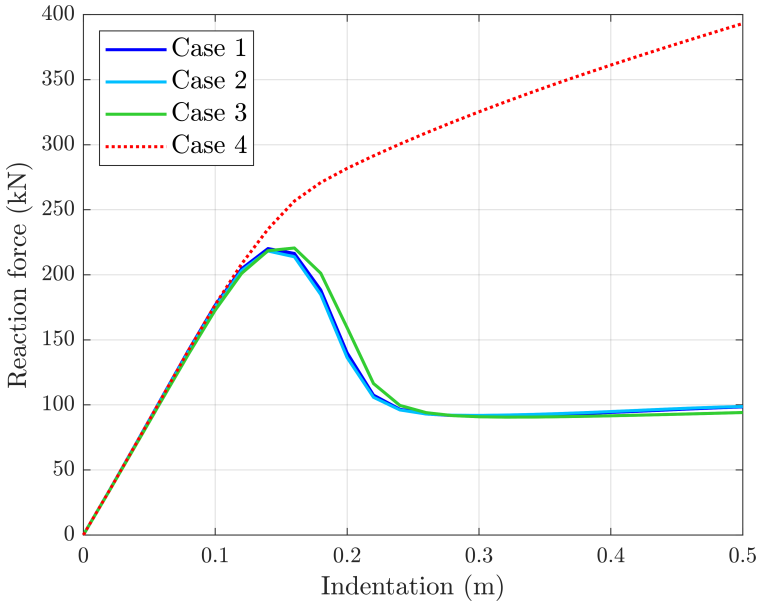

Figure 5: Reaction force vs. vertical displacement curve.

Q 2.6 *Section 4.4 first sentence, is this a verification example or validation example?*

Reply: Thank you for your comment. From our understanding of the difference between "verification" and "validation": "validation" is the process of checking whether the model captures the physics of the real problem (always compare with laboratory experiments), while "verification" is the process of checking that the software works correctly. Therefore, the word "verification" is preferred here.

Q 2.7 *Page 17 line 16, "It is worth mentioning that ..."*

Reply: We have corrected this grammar error. Thank you.

Q 2.8 *Page 17 line 22, it is not necessary to abbreviate DOS if it is not used in other places.*

Reply: Thank you for your comment. We have deleted this abbreviation.

Reviewer 3

We didn't receive the comments from Reviewer #3.

Reviewer 4

Q 4.1 *There are two aspects in the manuscript that were noted by the authors: (1) a new poroelastoplastic formulation for anisotropic material with a double porosity structure, and (2) a stabilized NS-FEM element for analysis of problems described in (1). Before this paper can go through, the authors need to address the following points.*

Reply: Thank you for your brief summary that directly pointed out the essential findings of this work.

Q 4.2 *State clearly what is gained from the new poroelastoplastic formulation for anisotropic material with a double porosity structure. The authors have done a good job at the background literature, but it is not clear to the reviewer how the proposed new formulation differs from those already found in the literature. Is it the case where the equations were written in different forms but are essentially the same as those already presented in the literature, or is there an additional physics included in the present formulation that is not found in previous work? Please elaborate.*

Reply: Thank you for your insightful comment. The new formulation is not simply a revisit of the previous formulations (written in different forms), it actually allows us to capture additional physics: the nature of anisotropy for each material and differences among various materials' stiffness. Take the more general multiple porosity media as an example that is mentioned by Reviewer #1, in our formulation, we allow N poroelastic constituents to be anisotropic, as shown in Figure 6 modified from Mehrabian and Abousleiman (2014). In the original work of Mehrabian and Abousleiman (2014), only isotropic poroelastic constituents were considered. The extension of our double porosity formulation to this scenario of multiple porosity has been discussed in our response to Reviewer #1.

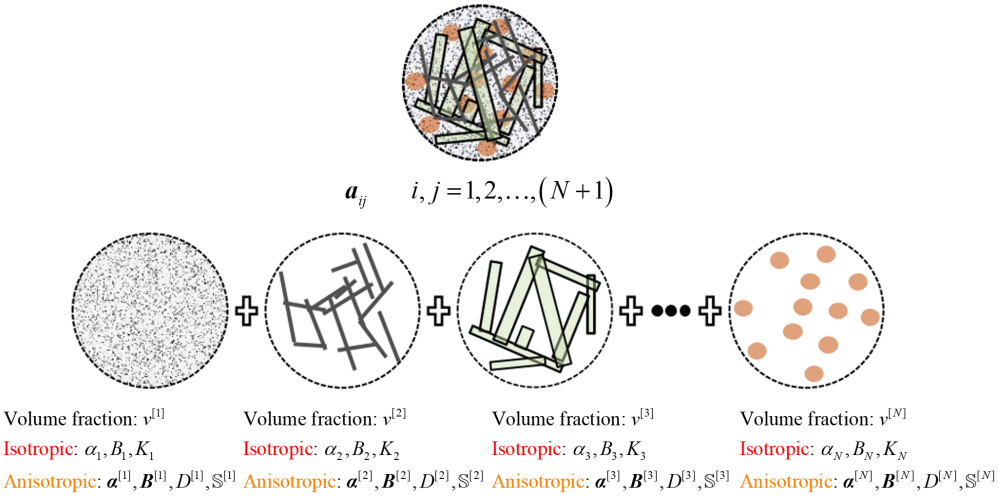

Figure 6: N poroelastic constituents comprising a N porosity poroelastic mixture with mechanical properties $\boldsymbol{a}_{ij}$ (Mehrabian and Abousleiman, 2014). The additional physics of anisotropy is considered in our proposed formulation, which is not discussed in Mehrabian and Abousleiman (2014).

Another novel finding is that we would have a better understanding of the significance of $\mathcal{C}$ proposed by Zhang and Borja (2021). The formulation given by Zhang and Borja (2021) can be derived as a special case of the current formulation when two materials are assigned with the same solid and fluid properties. Under this assumption, the pore fractions ψ^m and ψ^M defined in Zhang and Borja (2021) are equal to $v^{[1]}$

and $v^{[2]}$, respectively. Also, the materials 1 and 2 are identical to the nanopore matrix (skeleton) and the micro-fracture matrix (skeleton), respectively. It is necessary to mention that two materials have the same intrinsic porosity ϕ. After some algebraic manipulations, the final results from the proposed formulation are given as follows. The Biot tensors $\boldsymbol{\alpha}_1 = v^{[1]}\boldsymbol{\alpha}$ and $\boldsymbol{\alpha}_2 = v^{[2]}\boldsymbol{\alpha}$ take the same form as Zhang and Borja (2021). For storage coefficients, they adopt the following values

$$A_{11} = v^{[1]}v^{[2]}D + \frac{v^{[1]}v^{[1]}}{\mathcal{M}} = \frac{\beta v^{[1]}v^{[1]}}{K_s} + \frac{\phi v^{[1]}}{K_f} + v^{[1]}v^{[2]}\left(C_K^* - \frac{1+\phi}{K_s}\right), \tag{12}$$

$$A_{22} = v^{[1]}v^{[2]}D + \frac{v^{[2]}v^{[2]}}{\mathcal{M}} = \frac{\beta v^{[2]}v^{[2]}}{K_s} + \frac{\phi v^{[2]}}{K_f} + v^{[1]}v^{[2]}\left(C_K^* - \frac{1+\phi}{K_s}\right), \tag{13}$$

$$A_{12} = -v^{[1]}v^{[2]}\left(D - \frac{1}{\mathcal{M}}\right) = \frac{\beta v^{[1]}v^{[2]}}{K_s} - v^{[1]}v^{[2]}\left(C_K^* - \frac{1+\phi}{K_s}\right), \tag{14}$$

where β is defined in Eq. (35) of Zhang and Borja (2021) and $C_K^* = S_{iijj}$ (recall $\mathbb{S}$ is the drained elastic compliance tensor) is defined by Cheng (2016). By comparing above three equations with Eq. (73) of Zhang and Borja (2021) and noting that $\phi^m = \phi v^{[1]}$ and $\phi^M = \phi v^{[2]}$, an important relation is obtained

$$\frac{\phi}{\mathcal{C}} = v^{[1]}v^{[2]}\left(C_K^* - \frac{1+\phi}{K_s}\right). \tag{15}$$

Equation (15) bridges the two formulations in a perfect way since by comparing Eq. (15) with Eq. (66) of Zhang and Borja (2021), $1/K_m^e$ and $1/K_M^e$ (Zhang and Borja, 2021) are replaced by the generalized compressibility C_K^*, and K_s is contained in the expression of b in Zhang and Borja (2021). These excellent correspondences suggest the validity of **both** formulations.

However, in the real situation, two materials usually have different stiffness and porosity (Yan et al., 2018). In general, the joint phase (natural fracture) has a higher intrinsic porosity and a lower stiffness than the matrix phase. Therefore, in Section 3 we have re-calculated the poroelastic coefficients of the Weber sandstone by considering above factors, which also indicates more clear physics. This detailed calculation spreadsheet is also suggested by Reviewer #1. We hope this thorough comparison could make you satisfied and thank you for your approval.

The revised contents could be found in Section 2.1 and Section 3.

Q 4.3 *As for the stabilized NS-FEM, how does this approach compare with the stabilized finite elements presented in Reference 61? The reviewer realizes that T3 elements are involved in the present work, whereas bi-linear elements were used in Reference 61. However, it appears that the amount of computation involved does not fully justify the proposed approach, not to mention the fact that the formulation does not look as appealing as the one presented in Reference 61. Just looking at Figure 1, the extra work implied by the smoothing domain (yellow region) is a turn-off for most code developers. Why insist on using T3 elements? More justification is needed here.*

Reply: Thank you for your insightful comment. The justifications of the smoothing operation, the use of T3 element, and the computational efficiency are shown in the following bullet form.

- The node-based smoothing domain is automatically generated from a triangular mesh without any human interventions (Liu and Nguyen, 2010). Only edge midpoints and element centroids are needed in this generation process.

- Although the shape of the smoothing domain (SD) looks irregular in Figure 1, the smoothed strain-displacement matrix $\bar{\mathbb{B}}$ is a constant over this SD. Therefore, in the assembly process, the quadrature

points of this SD are not needed, as supported by the first term of Eq. (40). All the relevant information is stored in the **nodes** instead of quadrature points, thus the cost for variable mapping between nodes and quadrature points for FEM is not needed. This is extremely helpful in the large deformation analysis that requires re-meshing strategy (Jin et al., 2021a,b; Wang et al., 2022). For T3 element, the calculation of $\bar{\mathbb{B}}$ and $\bar{\mathbb{E}}$ only involves arithmetic weighting average, while for other elements, the calculation requires boundary integration, which is more difficult for code implementation.

- The reason that the T3 element is adopted is because of the evaluation of the modified nodal integration term, as shown in Eq. (43). In a meshfree interpolation scheme, extra evaluation of (smoothed) gradient at each additional stress point is unavoidable (Wei et al., 2016). However, due to the linear shape function and its piecewise constant derivatives in NS-FEM, these counterparts just take the same value as the compatible gradient matrices $\tilde{\mathbb{B}}$ that have been calculated beforehand, so that no extra computational effort is required, which favors the use of T3 element.

- Compared with the stabilized finite element presented in [61], the useful PPP technique is also adopted in our approach (but for T3 element), as shown in Eqs. (50)(51). The difference is in the modified nodal integration term Eq. (43) that has been calculated in the preprocessing script, and its effect has been illustrated in Figure 15 of our manuscript. In addition, for T3 element, the assembly of the PPP term is very simple since the contribution from each triangle element is purely a constant matrix multiplied by the element area.

- The T3 element is also a good candidate for unstructured mesh (especially with explicit fractures) and local mesh refinement, as shown in Figures 8 and 17 in Wang et al. (2022) and Figure 3 in Jiang and Yang (2018).

- As for the amount of computation, Figure 13 of Wang et al. (2022) already illustrates the computational efficiency of NS-FEM, compared with the standard FEM. The NS-FEM has the lowest computational time while the results accuracy is still as good as the traditional FEM, as shown in Figure 9 of Wang et al. (2022). Although the formulation in Section 3 does not look as appealing as that in [61], the actual implementation is easier than it feels like. We have made our code publicly available from this GitHub page under the **Releases** menu, in which you could find the main file is much shorter than the C++ code built on the deal.II library. Furthermore, all the numerical examples used in this manuscript could be computed in a reasonable amount of time (less than 15 minutes).

The revised content could be found in Section 4.

Q 4.4 *The presentation can also be improved. The reviewer suggests to tone down loose and ambiguous sentences aimed to "sell" their model. For example, in the Abstract the authors state in their last sentence that "the anisotropic elastoplastic response, etc., can only be captured through this proposed robust computational model." This is an exaggerated statement that the reviewer does not support. On line 5 of page 28, the authors claim that their formulation is more reliable. What do they mean by "reliable"? In the same section, they claim that the obtained results are "reasonable". Again, this is a very loose statement that must be edited. Just stick to the facts and avoid all these unnecessary exaggerations that do not help the cause of the paper.*

Reply: Thank you for your comment. We have carefully rewritten these ambiguous and exaggerated sentences and just focus on the numerical facts.

Q 4.5 *In the first paragraph of page 2, the authors state that a constant binary fraction of porosity was always adopted by previous work and that a new parameter C was derived in Reference 21, but this new parameter "is difficult to measure." The reviewer disagrees. Nothing can be easier to determine than a parameter that is*

derived from one-dimensional consolidation tests, please see Figures 3 and 5 of Reference 21. Furthermore, the authors state that "the effective stress partition assumption is not validated", but this reviewer does not see how the authors validated their effective stress either. The word "validate" implies comparison with experiments. What experiments did the authors use to validate their model? There was not a single experiment presented in the paper.

Reply: Thank you for your comment. You are definitely correct that there is also no experiment in this manuscript to validate the theory in Section 2. We have carefully modified our description of the prominent work [21]. Hope you are satisfied with the new description.

Q 4.6 *The reviewer suggests that the authors choose a different symbol for C in Equation (2) so as not to confuse it with the moduli tensor.*

Reply: Thank you for your advice. We have changed the symbol C to D to represent the constant stress storage coefficient.

Q 4.7 *Line 37 of page 4: "fluid flow and mechanics" is a meaningless phrase. Fluid flow is also mechanics, as in fluid mechanics. State "solid deformation" in lieu of mechanics.*

Reply: Thank you for pointing out this meaningless phrase. We have modified it accordingly.

Q 4.8 *The manuscript was written in first, second, and third persons. Sometimes, the authors use "you" (line 16 of page 5), sometimes "we" (line 46 of page 5), and sometimes, passive sentences. Please be consistent and avoid the second person.*

Reply: Thank you for your advice. The grammatical person is now consistent in the revised work.

Q 4.9 *Note that adjectives qualify nouns and adverbs qualify adjectives. Adjectives cannot qualify adjectives and nouns cannot qualify nouns. So, "non-overlapping subdomains" and not "non-overlap subdomains" (appearing numerous times); "transversely isotropic" and not "transverse isotropic" (Figure 2 caption); etc. Line 4 on page 12: "satisfactory result" and not "satisfying result". Line 6 of the same paragraph: "are given". On line 5 of page 14, what do the authors mean by "non-dimensionalization"?*

Reply: Thank you for providing this nice instruction. All of these grammar errors have been corrected. The term "non-dimensionalization" implies the PDEs are written in dimensionless form. During the revision, it seems that this term is not very important, so this ambiguous and long term has been deleted.

Q 4.10 *On line 5 of page 17, the authors incorrectly attributed the AMCC model to Reference 80, but it was actually developed in Reference 84.*

Reply: Thank you for pointing out this error. We have now attributed the AMCC model to the correct reference.

Q 4.11 *The zigzag pattern mentioned on line 35 of page 17 has been explained in the context of sliding along bedding planes in the additional Reference 1 (Zhao and Borja, 2022) below.*

Reply: Thank you for providing this excellent paper. We have added this explanation to the corresponding paragraph and cited this work.

Q 4.12 *In Table 5, it's not a good idea to tabulate a matrix. Enter the components of the matrix (or tensor) instead of the matrix itself.*

Reply: Thank you for your comment. We have now entered the components of the matrix (or tensor) in Tables.

Q 4.13 *Figure 20 is too dense. There has to be a better way of presenting the results in a less confusing manner.*

Reply: Thank you for your comment. Figure 20 is now replaced by four sub-figures, which is much more clear.

Q 4.14 *Reference 2 (Camargo et al., 2021) below could be another useful reference on stabilization in the context of finite element-finite volume approach.*

Reply: Thank you for providing this excellent paper. We have added relevant descriptions and cited this work.

Q 4.15 *And finally, please embed the figures in the text. Most reviewers now review manuscripts directly on their laptop screens instead of printing them. As a courtesy to reviewers, please make the reviewing process more manageable to them by sparing them the task of flipping their laptop screens back and forth just to see the figures.*

Reply: Thank you for your kind comment. The figures are now embedded in the text.

References

R. I. Borja. *Plasticity*. Springer Berlin Heidelberg, Berlin, Heidelberg, 2013. doi: 10.1007/978-3-642-38547-6.

J. T. Camargo, J. A. White, and R. I. Borja. A macroelement stabilization for mixed finite element/finite volume discretizations of multiphase poromechanics. *Computational Geosciences*, 25(2):775–792, Apr. 2021. doi: 10.1007/s10596-020-09964-3.

A. H. D. Cheng. *Poroelasticity*. Springer Science+Business Media, New York, NY, 2016. ISBN 978-3-319-25200-1.

H. Feng, X. Y. Cui, and G. Y. Li. A stable nodal integration method with strain gradient for static and dynamic analysis of solid mechanics. *Engineering Analysis with Boundary Elements*, 62:78–92, Jan. 2016. doi: 10.1016/j.enganabound.2015.10.001.

J. Jiang and J. Yang. Coupled fluid flow and geomechanics modeling of stress-sensitive production behavior in fractured shale gas reservoirs. *International Journal of Rock Mechanics and Mining Sciences*, 101:1–12, Jan. 2018. doi: 10.1016/j.ijrmms.2017.11.003.

Y.-F. Jin, Z.-Y. Yin, J. Li, and J.-G. Dai. A novel implicit coupled hydro-mechanical SPFEM approach for modelling of delayed failure of cut slope in soft sensitive clay. *Computers and Geotechnics*, 140:104474, Dec. 2021a. doi: 10.1016/j.compgeo.2021.104474.

Y.-F. Jin, Z.-Y. Yin, X.-W. Zhou, and F.-T. Liu. A stable node-based smoothed PFEM for solving geotechnical large deformation 2D problems. *Computer Methods in Applied Mechanics and Engineering*, 387:114179, Dec. 2021b. doi: 10.1016/j.cma.2021.114179.

J. Kim, E. L. Sonnenthal, and J. Rutqvist. Formulation and sequential numerical algorithms of coupled fluid/heat flow and geomechanics for multiple porosity materials. *International Journal for Numerical Methods in Engineering*, 92(5):425–456, Nov. 2012. doi: 10.1002/nme.4340.

G.-R. Liu and T. T. Nguyen. *Smoothed finite element methods*. Taylor & Francis, Boca Raton, 2010. ISBN 978-1-4398-2027-8.

A. Mehrabian and Y. N. Abousleiman. Generalized Biot's theory and Mandel's problem of multiple-porosity and multiple-permeability poroelasticity. *Journal of Geophysical Research: Solid Earth*, 119(4):2745–2763, Apr. 2014. doi: 10.1002/2013JB010602.

W. Sun, J. T. Ostien, and A. G. Salinger. A stabilized assumed deformation gradient finite element formulation for strongly coupled poromechanical simulations at finite strain. *International Journal for Numerical and Analytical Methods in Geomechanics*, 37(16):2755–2788, Nov. 2013. doi: 10.1002/nag.2161.

Z.-Y. Wang, Y.-F. Jin, Z.-Y. Yin, and Y.-Z. Wang. A novel coupled NS-PFEM with stable nodal integration and polynomial pressure projection for geotechnical problems. *International Journal for Numerical and Analytical Methods in Geomechanics*, 46(13):2535–2560, Sept. 2022. doi: 10.1002/nag.3417.

H. Wei, J.-S. Chen, and M. Hillman. A stabilized nodally integrated meshfree formulation for fully coupled hydro-mechanical analysis of fluid-saturated porous media. *Computers & Fluids*, 141:105–115, Dec. 2016. doi: 10.1016/j.compfluid.2015.11.002.

X. Yan, Z. Huang, J. Yao, Y. Li, D. Fan, and K. Zhang. An efficient hydro-mechanical model for coupled multi-porosity and discrete fracture porous media. *Computational Mechanics*, 62(5):943–962, Nov. 2018. doi: 10.1007/s00466-018-1541-5.

H. Yang, X. Y. Cui, S. Li, and Y. H. Bie. A stable node-based smoothed finite element method for metal forming analysis. *Computational Mechanics*, 63(6):1147–1164, June 2019. doi: 10.1007/s00466-018-1641-2.

Z.-Y. Yin, M. Karstunen, C. S. Chang, M. Koskinen, and M. Lojander. Modeling Time-Dependent Behavior of Soft Sensitive Clay. *Journal of Geotechnical and Geoenvironmental Engineering*, 137(11):1103–1113, Nov. 2011. doi: 10.1061/(ASCE)GT.1943-5606.0000527.

W. Zeng and G. R. Liu. Smoothed Finite Element Methods (S-FEM): An Overview and Recent Developments. *Archives of Computational Methods in Engineering*, 25(2):397–435, Apr. 2018. doi: 10.1007/s11831-016-9202-3.

Q. Zhang and R. I. Borja. Poroelastic coefficients for anisotropic single and double porosity media. *Acta Geotechnica*, 16(10):3013–3025, Apr. 2021. doi: 10.1007/s11440-021-01184-y.

Q. Zhang, X. Yan, and J. Shao. Fluid flow through anisotropic and deformable double porosity media with ultra-low matrix permeability: A continuum framework. *Journal of Petroleum Science and Engineering*, 200:108349, May 2021. doi: 10.1016/j.petrol.2021.108349.

Y. Zhao and R. I. Borja. Anisotropic elastoplastic response of double-porosity media. *Computer Methods in Applied Mechanics and Engineering*, 380:113797, July 2021. doi: 10.1016/j.cma.2021.113797.

Y. Zhao and R. I. Borja. A double-yield-surface plasticity theory for transversely isotropic rocks. *Acta Geotechnica*, 2022. doi: 10.1007/s11440-022-01605-6.

Y. Zhao, S. J. Semnani, Q. Yin, and R. I. Borja. On the strength of transversely isotropic rocks. *International Journal for Numerical and Analytical Methods in Geomechanics*, 42(16):1917–1934, Nov. 2018. doi: 10.1002/nag.2809.

Supplementary material for

A novel stabilized NS-FEM formulation for anisotropic double porosity media

Qi Zhang[1], Ze-Yu Wang[1], Zhen-Yu Yin[1], and Yin-Fu Jin[1,2]

[1]Department of Civil and Environmental Engineering, The Hong Kong Polytechnic University, Hung Hom, Kowloon, Hong Kong, China
[2]College of Civil and Transportation Engineering, Shenzhen University, Shenzhen, China

This supplementary material is based on the following three references.

1. Semnani, S.J., White, J.A., Borja, R.I., 2016. Thermoplasticity and strain localization in transversely isotropic materials based on anisotropic critical state plasticity. Int. J. Numer. Anal. Meth. Geomech. 40, 2423–2449.

2. Zhao, Y., Semnani, S.J., Yin, Q., Borja, R.I., 2018. On the strength of transversely isotropic rocks. Int. J. Numer. Anal. Meth. Geomech. 42, 1917–1934.

3. Zhang, Q., 2020. Hydromechanical modeling of solid deformation and fluid flow in the transversely isotropic fissured rocks. Computers and Geotechnics 128, 103812.

1 Review of the anisotropic modified Cam-Clay plasticity (AMCC) model for layered material

The elastic tensor $\mathbb{C}^e$ is transversely isotropic due to the existence of the bedding plane, which has the following expression

$$\begin{aligned}\mathbb{C}^e = {} & \lambda^e \mathbf{1}\otimes\mathbf{1} + 2\mu_T \mathbb{I} + a^e\left(\mathbf{1}\otimes\boldsymbol{M} + \boldsymbol{M}\otimes\mathbf{1}\right) \\ & + b^e \boldsymbol{M}\otimes\boldsymbol{M} + 2\left(\mu_L - \mu_T\right)\left(\boldsymbol{M}\odot\mathbf{1} + \mathbf{1}\odot\boldsymbol{M}\right),\end{aligned} \tag{1}$$

where $\mathbf{1}$ is the second-order identity tensor, $\mathbb{I} = \delta_{ik}\delta_{jl}\,\mathbf{e}_i\otimes\mathbf{e}_j\otimes\mathbf{e}_k\otimes\mathbf{e}_l$ is the fourth-order identity tensor, $(\boldsymbol{A}\odot\boldsymbol{B})_{ijkl} = A_{ik}B_{jl}$, $\boldsymbol{M} = \mathbf{n}\otimes\mathbf{n}$, $\mathbf{n}$ is the unit normal vector of the bedding plane, λ^e, μ_L, μ_T, a^e, and b^e are the material elastic constants. The subscript $(\cdot)_T$ means in the isotropic plane and subscript $(\cdot)_L$ means perpendicular to this isotropic plane. It is necessary to mention that when $\mathbf{n} = \mathbf{e}_z = [0,0,1]^T$, the Voigt form of $\mathbb{C}^e$ is given by the following 6 by 6 matrix C^e

$$C^e = \begin{bmatrix} \lambda^e+2\mu_T & \lambda^e & \lambda^e+a^e & & & \\ \lambda^e & \lambda^e+2\mu_T & \lambda^e+a^e & & & \\ \lambda^e+a^e & \lambda^e+a^e & \lambda^e+2\tilde{\mu} & & & \\ & & & \mu_T & & \\ & & & & \mu_L & \\ & & & & & \mu_L \end{bmatrix}, \tag{2}$$

where $\tilde{\mu} = 2\mu_L - \mu_T + a^e + b^e/2$. The generalized bulk modulus K^* for the drained transversely isotropic material is given as

$$K^* = \frac{\mathbf{1} : \mathbb{C}^e : \mathbf{1}}{9} = \lambda^e + \frac{2}{9}\mu_T + \frac{4}{9}\mu_L + \frac{2}{3}a^e + \frac{1}{9}b^e \,. \tag{3}$$

The yield function f is given as

$$f(\boldsymbol{\sigma}, p_c) = \frac{\boldsymbol{\sigma} : \mathbb{A} : \boldsymbol{\sigma}}{2M^2} + (\boldsymbol{a} : \boldsymbol{\sigma})(\boldsymbol{a} : \boldsymbol{\sigma} - p_c) \,, \tag{4}$$

where $\mathbb{A} = \mathbb{P} : (3\mathbb{I} - \mathbf{1} \otimes \mathbf{1}) : \mathbb{P}$, and $\mathbb{P} = c_1^p \mathbb{I} + c_2^p \boldsymbol{M} \odot \boldsymbol{M} + c_3^p (\boldsymbol{M} \odot \mathbf{1} + \mathbf{1} \odot \boldsymbol{M})/2$ is the stress projection tensor, c_1^p, c_2^p, and c_3^p are the projection constants, $\boldsymbol{a} = \mathbb{P} : \mathbf{1}/3$, $M = 6\sin\phi_{cs}/(3 - \sin\phi_{cs})$ is the non-zero slope of the critical state line, ϕ_{cs} is the critical state friction angle, $p_c < 0$ is the preconsolidation pressure. Note when $\mathbb{P} = \mathbb{I}$, the yield function would retreat to the standard yield function of MCC. After specifying the yield function f, the plastic strain increment $\mathrm{d}\boldsymbol{\epsilon}^p = \mathrm{d}\boldsymbol{\epsilon} - \mathrm{d}\boldsymbol{\epsilon}^e$ can be calculated using the associative flow rule as

$$\mathrm{d}\boldsymbol{\epsilon}^p = \mathrm{d}\lambda \frac{\partial f}{\partial \boldsymbol{\sigma}} = \mathrm{d}\lambda \left[\frac{\mathbb{A} : \boldsymbol{\sigma}}{M^2} + \boldsymbol{a}(2\boldsymbol{a} : \boldsymbol{\sigma} - p_c) \right] , \tag{5}$$

where $\mathrm{d}\lambda \geq 0$ is the plastic scalar multiplier. The last component of this model is the hardening law for p_c, which is given as

$$\mathrm{d}p_c = \frac{p_c}{\lambda^p} \mathrm{d}\epsilon_v^p \,, \tag{6}$$

where $\mathrm{d}\epsilon_v^p = \mathrm{Tr}(\mathrm{d}\boldsymbol{\epsilon}^p)$ and $\lambda^p < 0$ is the plastic compressibility parameter.

2 Return mapping algorithm and algorithmic stress-strain tangent operator

The return mapping algorithm starts by backward Euler integrating plasticity equations (in rate form) from time t_n to t_{n+1}, and a group of coupled equations with unknowns $\boldsymbol{\sigma}$, $\Delta\lambda$, and p_c could be obtained

$$-\left(\boldsymbol{\sigma}^{\mathrm{old}} + \mathbb{C}^e : \Delta\boldsymbol{\epsilon}\right) + \mathbb{C}^e : \left(\Delta\lambda \frac{\partial f}{\partial \boldsymbol{\sigma}}\right) + \boldsymbol{\sigma} = \mathbf{0} \,, \tag{7}$$

$$p_c^{\mathrm{old}} \exp\left[\frac{\Delta\lambda\, \mathrm{Tr}(\partial f/\partial\boldsymbol{\sigma})}{\lambda^p}\right] - p_c = 0 \,, \tag{8}$$

$$f(\boldsymbol{\sigma}, p_c) = 0 \,, \tag{9}$$

where the superscript marks old physical variables, and all the other physical variables are at time t_{n+1}.

The second step of the return mapping algorithm is to check whether plastic deformation could accumulate. First of all, trial solutions are constructed as $\boldsymbol{\sigma}^{\mathrm{trial}} = \boldsymbol{\sigma}^{\mathrm{old}} + \mathbb{C}^e : \Delta\boldsymbol{\epsilon}$ and $p_c^{\mathrm{trial}} = p_c^{\mathrm{old}}$. Next, the trial solutions are substituted into the yield function f. Finally, if $f \leq 0$, then we are in the elastic range and we don't need to solve above coupled equations, the $\mathbb{C}^{\mathrm{algo}}$ is equal to the $\mathbb{C}^e$, otherwise, we proceed to the third step.

In the third step, pure Newton's method is applied to solve above coupled equations simultaneously provided $f > 0$. To illustrate this method more efficiently, full matrix/vector notation is adopted, see Section 3. Following this notation, $x \in \mathbb{R}^9$, $y \in \mathbb{R}$, and $z \in \mathbb{R}$ are used to represent $\boldsymbol{\sigma}$, $\Delta\lambda$, and p_c, respectively. Also, the original $\mathbb{C}^e$ is transformed to symmetric $C^e \in \mathbb{R}^{9\times 9}$, the fourth-order identity tensor $\mathbb{I}$ is transformed to identity matrix $I \in \mathbb{R}^{9\times 9}$, the second-order identity tensor $\mathbf{1}$ is transformed to $I_2 \in \mathbb{R}^9$,

$\boldsymbol{\sigma}^{\text{trial}}$ is transformed to $\sigma^{\text{trial}} \in \mathbb{R}^9$, $\mathbb{A}$ is transformed to symmetric $A \in \mathbb{R}^{9\times 9}$, and $\boldsymbol{a}$ is transformed to $a \in \mathbb{R}^9$. In Newton's method, the residual vector $g \in \mathbb{R}^{11}$ and Hessian matrix $J \in \mathbb{R}^{11\times 11}$ are constructed for every iteration. Suppose the superscript v with parentheses is used to represent iteration counter where $v = 0$ means the initial guess, then for each v, we need to solve following block linear equations to obtain the Newton's step $\left[\delta x^T, \delta y, \delta z\right]^T$ and update $\left[x^{(v+1)^T}, y^{(v+1)}, z^{(v+1)}\right]^T = \left[x^{(v)^T}, y^{(v)}, z^{(v)}\right]^T + \left[\delta x^T, \delta y, \delta z\right]^T$ for next iteration

$$\begin{bmatrix} J_{11}^{(v)} & J_{12}^{(v)} & J_{13}^{(v)} \\ J_{21}^{(v)} & J_{22}^{(v)} & J_{23}^{(v)} \\ J_{31}^{(v)} & J_{32}^{(v)} & J_{33}^{(v)} \end{bmatrix} \begin{bmatrix} \delta x \\ \delta y \\ \delta z \end{bmatrix} = \begin{bmatrix} -g_1^{(v)} \\ -g_2^{(v)} \\ -g_3^{(v)} \end{bmatrix}, \tag{10}$$

where $g_1^{(v)} \in \mathbb{R}^9$, $g_2^{(v)} \in \mathbb{R}$, and $g_3^{(v)} \in \mathbb{R}$ are block vectors of the residual vector g, $J_{11}^{(v)} \in \mathbb{R}^{9\times 9}$, $J_{12}^{(v)} \in \mathbb{R}^{9\times 1}$, $J_{13}^{(v)} \in \mathbb{R}^{9\times 1}$, $J_{21}^{(v)} \in \mathbb{R}^{1\times 9}$, $J_{22}^{(v)} \in \mathbb{R}$, $J_{23}^{(v)} \in \mathbb{R}$, $J_{31}^{(v)} \in \mathbb{R}^{1\times 9}$, $J_{32}^{(v)} \in \mathbb{R}$, and $J_{33}^{(v)} \in \mathbb{R}$ are block matrices of the Hessian matrix J. The expressions for these block elements are given in Section 4.

In the last step of the return mapping algorithm, when the stopping criterion is satisfied, we are ready to use the updated $\boldsymbol{\sigma}$, $\Delta\lambda$, and p_c (same as $x^{(\text{last})}$, $y^{(\text{last})}$, and $z^{(\text{last})}$) to calculate $\mathbb{C}^{\text{algo}}$ in the 9×9 matrix form C^{algo}. The procedure is given here. First of all, $x_1 \in \mathbb{R}^9$ and $x_2 \in \mathbb{R}^9$ are solved such that they satisfy following linear equations (18×18)

$$\begin{bmatrix} \left(J_{21}J_{11}^{-1}J_{12} - J_{22}\right) I & \left(J_{21}J_{11}^{-1}J_{13} - J_{23}\right) I \\ \left(J_{31}J_{11}^{-1}J_{12}\right) I & \left(J_{31}J_{11}^{-1}J_{13} - J_{33}\right) I \end{bmatrix} \begin{bmatrix} x_1 \\ x_2 \end{bmatrix} = \begin{bmatrix} \left(J_{21}J_{11}^{-1}C^e\right)^T \\ \left(J_{31}J_{11}^{-1}C^e\right)^T \end{bmatrix}. \tag{11}$$

As mentioned before, J is evaluated at the termination of the Newton's method. After obtaining x_1 and x_2, C^{algo} can be calculated easily as

$$C^{\text{algo}} = J_{11}^{-1}C^e - J_{11}^{-1}J_{12}x_1^T - J_{11}^{-1}J_{13}x_2^T. \tag{12}$$

It is also necessary to mention that although the analytical formula for $\mathbb{C}^{\text{algo}}$ is derived, it is given in the full 9×9 matrix form (C^{algo}), thus a transformation to the traditional 6×6 matrix form is necessary, please see Section 3 for more details.

As a final note of this section, in Section 5, the complete calculation results of a typical uniaxial strain point simulation in 3D after 5 incremental loading steps with the same $\Delta\boldsymbol{\epsilon}$ is provided. Any other return mapping algorithms should be able to reproduce exactly the same results before they are used in real problems.

3 Full matrix/vector notation

In this notation, the second-order tensors such as stress and strain are stored in column vectors such as $x \in \mathbb{R}^9$, and the fourth-order tensors are stored in matrices such as $C \in \mathbb{R}^{9\times 9}$, thus the transformation rule needs to be stated, *i.e.*, the correspondence $\alpha \leftrightarrow ij$ and $\beta \leftrightarrow kl$ where $\alpha, \beta = 1, 2, \ldots, 9$ and $i, j, k, l = 1, 2, 3$, see following Table 1. Given a 9×9 stiffness matrix C, the aim is to output the equivalent 6×6 stiffness matrix $\hat{C}$. To accomplish that, a matrix $E \in \mathbb{R}^{9\times 6}$ is defined as follows

$$E = \begin{bmatrix} e_1 & e_5 & e_9 & (e_2 + e_4)/2 & (e_3 + e_7)/2 & (e_6 + e_8)/2 \end{bmatrix}, \tag{13}$$

where $e_i \in \mathbb{R}^9$ for $i = 1, 2, \ldots, 9$ are unit vectors in the 9 dimensional space, and e_i means that only the i^{th} component is 1, all the other components are 0. Next we do the matrix multiplication and obtain $B = CE$

Table 1: Transformation rule.

Vector indices α and β	1	2	3	4	5	6	7	8	9
Tensor index pairs ij and kl	11	21	31	12	22	32	13	23	33

that is also a 9×6 matrix. Let us rewrite B using row representations $b_j \in \mathbb{R}^6$ for $j = 1, 2, \ldots, 9$, now $\hat{C}$ is represented as

$$\hat{C} = \begin{pmatrix} b_1^T \\ b_5^T \\ b_9^T \\ b_4^T \\ b_7^T \\ b_8^T \end{pmatrix}, \tag{14}$$

which is a 6×6 matrix. Here the default order of the Voigt notation is 11, 22, 33, 12, 13, 23. In Cartesian coordinate system, the order is described as xx, yy, zz, xy, xz, yz. It is also important to mention that above procedure only applies to the stiffness matrix. For compliance matrix, please drop the "/2" in the first equation, and multiply the last three rows of $\hat{C}$ in the second equation by 2.

4 Residual vector and Hessian matrix for the return mapping algorithm

The following expressions are used in the Eq. (10)

$$g_1^{(v)} = x^{(v)} + y^{(v)} C^e \left[\frac{Ax^{(v)}}{M^2} + a \left(2a^T x^{(v)} - z^{(v)} \right) \right] - \sigma^{\text{trial}}, \tag{15}$$

$$g_2^{(v)} = p_c^{\text{old}} \exp \left[\frac{y^{(v)}}{\lambda^p} I_2^T \left(\frac{Ax^{(v)}}{M^2} + a \left(2a^T x^{(v)} - z^{(v)} \right) \right) \right] - z^{(v)}, \tag{16}$$

$$g_3^{(v)} = \frac{{x^{(v)}}^T A x^{(v)}}{2M^2} + a^T x^{(v)} \left(a^T x^{(v)} - z^{(v)} \right), \tag{17}$$

$$J_{11}^{(v)} = I + y^{(v)} C^e \left(\frac{A}{M^2} + 2aa^T \right), \tag{18}$$

$$J_{12}^{(v)} = C^e \left[\frac{Ax^{(v)}}{M^2} + a \left(2a^T x^{(v)} - z^{(v)} \right) \right], \tag{19}$$

$$J_{13}^{(v)} = -y^{(v)} C^e a, \tag{20}$$

$$J_{21}^{(v)} = \frac{y^{(v)} p_c^{\text{old}}}{\lambda^p} \exp \left[\frac{y^{(v)}}{\lambda^p} I_2^T \left(\frac{Ax^{(v)}}{M^2} + a \left(2a^T x^{(v)} - z^{(v)} \right) \right) \right] I_2^T \left(\frac{A}{M^2} + 2aa^T \right), \tag{21}$$

$$J_{22}^{(v)} = \frac{p_c^{\text{old}}}{\lambda^p} \exp \left[\frac{y^{(v)}}{\lambda^p} I_2^T \left(\frac{Ax^{(v)}}{M^2} + a \left(2a^T x^{(v)} - z^{(v)} \right) \right) \right] I_2^T \left[\frac{Ax^{(v)}}{M^2} + a \left(2a^T x^{(v)} - z^{(v)} \right) \right], \tag{22}$$

$$J_{23}^{(v)} = -\frac{y^{(v)} p_c^{\text{old}}}{\lambda^p} \exp\left[\frac{y^{(v)}}{\lambda^p} I_2^T \left(\frac{Ax^{(v)}}{M^2} + a\left(2a^T x^{(v)} - z^{(v)}\right)\right)\right] I_2^T a - 1\,, \tag{23}$$

$$J_{31}^{(v)} = \left[\frac{Ax^{(v)}}{M^2} + a\left(2a^T x^{(v)} - z^{(v)}\right)\right]^T\,, \tag{24}$$

$$J_{32}^{(v)} = 0\,, \tag{25}$$

$$J_{33}^{(v)} = -a^T x^{(v)}\,. \tag{26}$$

5 Benchmark strain point simulation

In this strain point simulation, we assume $\boldsymbol{a} = \mathbb{P} : \mathbf{1}/3$ and following material parameters that are similar to those of Tournemire shale: $\lambda^e = 4270$ MPa, $\mu_T = 9360$ MPa, $\mu_L = 6510$ MPa, $a^e = -1870$ MPa, $b^e = 5420$ MPa, $M = 1.07$, $\lambda^p = -0.0026$, $c_1^p = 0.7$, $c_2^p = -0.36$, and $c_3^p = 0.6$. The bedding plane angle is $\pi/3$ in $x\mathrm{O}y$ plane, which leads to $\mathbf{n} = \left[-\sqrt{3}/2, 1/2, 0\right]^T$ and following elastic stiffness matrix $\hat{C}^e \in \mathbb{R}^{6\times 6}$ (the default unit is MPa)

$$\hat{C}^e = \begin{bmatrix} 14683.75 & 3416.25 & 2867.50 & 1517.71 & 0 & 0 \\ 3416.25 & 19543.75 & 3802.50 & 2691.17 & 0 & 0 \\ 2867.50 & 3802.50 & 22990.00 & 809.73 & 0 & 0 \\ 1517.71 & 2691.17 & 809.73 & 7526.25 & 0 & 0 \\ 0 & 0 & 0 & 0 & 7222.50 & 1234.09 \\ 0 & 0 & 0 & 0 & 1234.09 & 8647.50 \end{bmatrix}. \tag{27}$$

For the stress history, the initial p_c is -40 MPa. The loading procedures are described as follows. First of all, the material is subject to an isotropic compression of -10 MPa, which leads to a non-zero initial strain, *i.e.*, $\boldsymbol{\epsilon}_0 \neq \mathbf{0}$. Next, we prescribe the same strain increment $\Delta\boldsymbol{\epsilon}$ at each step, and repeat it for 5 times. The $\Delta\boldsymbol{\epsilon}$ is given as

$$\Delta\boldsymbol{\epsilon} = \begin{bmatrix} 0 & 0 & 0 \\ 0 & -0.001 & 0 \\ 0 & 0 & 0 \end{bmatrix}. \tag{28}$$

That is to say, only axial deformation in the y-direction is allowed. As a result, only the first step is an elastic step and the other four steps are plastic steps. For benchmark verification, the final values of p_c, $\boldsymbol{\epsilon}$, $\boldsymbol{\sigma}$, and $\hat{C}^{\text{algo}} \in \mathbb{R}^{6\times 6}$ after 5 steps are provided here (the default unit is MPa except for $\boldsymbol{\epsilon}$)

$$p_c = -50.7379\,, \tag{29}$$

$$\boldsymbol{\epsilon} = \boldsymbol{\epsilon}_0 + 5\Delta\boldsymbol{\epsilon} = 10^{-3} \times \begin{bmatrix} -0.55858 & 0.14330 & 0 \\ 0.14330 & -5.39311 & 0 \\ 0 & 0 & -0.31038 \end{bmatrix}, \tag{30}$$

$$\boldsymbol{\sigma} = \begin{bmatrix} -35.87171 & -10.03319 & 0 \\ -10.03319 & -68.64135 & 0 \\ 0 & 0 & -39.60607 \end{bmatrix}, \tag{31}$$

$$\hat{C}^{\text{algo}} = \begin{bmatrix} 10992.87 & 4912.10 & 3186.54 & 1191.42 & 0 & 0 \\ 6238.00 & 7999.32 & 6613.18 & 883.05 & 0 & 0 \\ 3134.83 & 5692.87 & 17526.77 & 895.95 & 0 & 0 \\ 1384.35 & 1290.07 & 1013.99 & 4991.39 & 0 & 0 \\ 0 & 0 & 0 & 0 & 4786.39 & 1097.03 \\ 0 & 0 & 0 & 0 & 1097.03 & 6053.13 \end{bmatrix}. \tag{32}$$

Here $\hat{C}^{\text{algo}}$ is not symmetric albeit the flow rule is associative. This is because of the form of the incremental hardening law Eq. (8). In addition, here the order of the Voigt notation is xx, yy, zz, xy, xz, yz.

6 Simulation code availability statement

We have made our code publicly available from this GitHub page under the **Releases** menu. Please remember to cite the corresponding paper if you use any of these codes for research or industrial purposes.